1)Digitally controlled analog proportional-integral-derivative (PID) controller for high-speed scanning probe microscopy

Maja Dukic,[1] Vencislav Todorov,[2] Santiago Andany,[1] Adrian P. Nievergelt,[1] Chen Yang,[1] Nahid Hosseini,[1] and Georg E. Fantner[1,a)]

[1]Laboratory for Bio- and Nano-Instrumentation, School of Engineering, Ecole Polytechnique Federale de Lausanne, Lausanne 1015, Switzerland
[2]Techproject EMC GmbH, Vienna 1230, Austria

[a)] georg.fantner@epfl.ch

Abstract

Nearly all scanning probe microscopes (SPMs) contain a feedback controller, which is used to move the scanner in direction of the z-axis in order to maintain a constant setpoint based on the tip-sample interaction. The most frequently used feedback controller in SPM is the proportional-integral (PI) controller. The bandwidth of the PI controller presents one of the speed limiting factors in high-speed SPM, where higher bandwidths enable faster scanning speeds and higher imaging resolution. Most SPM systems use digital signal processor based PI feedback controllers, which require analog-to-digital and digital-to-analog converters. These converters introduce additional feedback delays which limit the achievable imaging speed and resolution. In this paper we present a digitally controlled analog proportional-integral-derivative (PID) controller. The controller implementation allows tunability of the PID gains over a large amplification and frequency range, while also providing precise control of the system and reproducibility of the gain parameters. By using the analog PID controller, we were able to perform successful atomic force microscopy imaging of a standard silicon calibration grating at line rates up to several kHz.

Keywords

PID, controller, AFM, SPM, analog electronics, high-speed AFM, high-speed SPM

I. INTRODUCTION

Atomic force microscopy (AFM), a type of scanning probe microscopy (SPM), is one of the few techniques that enables us to inspect dynamics of processes on the micrometer to nanometer scale[1,2]. In recent years, high-speed AFM (HS-AFM) has developed into an active research area, allowing for observation of dynamic processes over short timescales[1,3–7]. HS-AFM was made possible by increasing the mechanical and electrical bandwidths of each of the individual components of the AFM system, such as the cantilever[8–10], the scanner[11–17] and feedback electronic components[11,13,18]. Most AFM systems contain a feedback controller, which controls the scanner movement in the z-direction in order to keep the deflection or amplitude of the cantilever constant during scanning. This is usually used in order to maintain a constant force between the cantilever tip and the sample, which prevents damaging the tip

and the sample. The most frequently used feedback controllers in AFM are the proportional-integral (PI) and the proportional-integral-derivative (PID) controller. The bandwidth of the feedback controller is one of the limiting factors in HS-AFM and in general in SPM, where higher bandwidths enable faster scanning speeds and higher resolution.

Most AFM systems use digital signal processor (DSP) based PI feedback controllers. In such digital implementation of the controller, the signal needs to be sampled and afterwards quantized by an analog-to-digital converter (ADC) before it is sent to the processor. In order to avoid aliasing of high-frequency signals, it is necessary to perform signal sampling at a frequency which is usually 10 to 20 times higher than the system's closed-loop bandwidth. Additionally, the signal should be low-pass filtered before sampling, by an anti-aliasing filter to further reduce aliasing. Once the digital processor has calculated the new control value, which in turn causes an additional delay, this value needs to be converted back into a voltage by a digital-to-analog converter (DAC) in order for it to be applied to the plant (z-scanner).

As such, all of ADCs, DACs and filters introduce additional delays in the AFM feedback loop that limit AFM scanning speed. Moreover, ADCs and DACs can introduce quantization noise, which can be reduced by using high precision converters. As a consequence, HS-AFMs would necessitate high performance ADCs, DACs and DSPs in order to provide high speed, low noise and high conversion precision[19]. These parameters increase cost, power consumption and the complexity of a controller. Nevertheless, even high performance digital PI/PID controllers provide a limited bandwidth. For instance, commercial AFM PI controllers usually have a bandwidth of just a few tens of kHz, which is not sufficient for HS-AFM imaging. The reason for this is that, while ADCs and DACs can reach giga-sampling rates, they still introduce the considerable amount of delay. Recently, the increased availability of field programmable gate arrays (FPGA) has led to their use in the implementation of various parts of AFM systems, including the PID controller[20]. Nevertheless, they suffer from the similar problems as their DSP based counterparts. Many other control approaches were also implemented, such as H-∞ controllers[21–23] along with various other algorithms of modern control theory[24–27]. However, such approaches generally lead to an increased complexity of the system and often do not allow for user input to fine-tune the control parameters optimally for each sample.

Compared to the digital implementation, analog PID controllers provide higher feedback loop bandwidth in their basic configuration while also eliminating noise issues present in digital implementations. As analog systems by their nature do not sample, the limitations on the bandwidth of the analog PID controller are far less restrictive. In the past years, advances in the realization of reconfigurable analog blocks led to field programmable analog array (FPAA) systems being used to successfully implement PID controllers for control of various physical processes[19,28] and for various control applications in AFM[17,29,30]. FPAA manufacturers even offer manually tunable PID control interfaces[31]. However, FPAAs use switched-capacitor circuits for feedback and are still quantised in time.

Analog PID controllers have already been successfully used in several high-speed AFM experiments. Kodera et al. state that they measured maximum 70 kHz AFM feedback bandwidth using their analog dynamic PID controller[32]. Schitter et al. used an analog PID controller with manual analog potentiometers for AFM imaging where they report an AFM feedback bandwidth of around 100 kHz.[14] Using a feed-forward approach Uchihashi et al. state that they measured 50 – 70 kHz AFM feedback bandwith, depending on the amplitude setpoint. Although using analog PID controllers is advantageous for tracking bandwidth, the main disadvantage of the solely analog implementation of the controller is its lack of precise control and parameter reproducibility. In this work we present a digitally controllable, analog PID controller which allows precise, reproducible control of the system, as well as allows for dynamic control of the PID parameters.

Combining digital control of the gain parameters with an analog controller design can provide a very precise and fast response controller. Ugodzinski et al.[33] developed a prototype of an analog PID controller where the digitally controlled parameters are set using compact digital potentiometers. While the device is characterized with electrical input, no bandwidth measurements are presented and the controller is not applied to controlling a plant. A commercial digitally controlled analog PID is available from Stanford Research Systems (SIM960) with a specified bandwidth of 100kHz.

In this paper, we present a high-speed digitally controlled analog PID controller which combines the best features from both the analog and the digital implementation. The controller allows tunability of the PID gains over a large frequency range, while also providing precise control of the system and reproducibility of the gain parameters. The precise gain control over a large gain and frequency bandwidth is an important feature of SPM feedback controller as feedback loop conditions can change dramatically from one experiment to another. By using our analog PID controller we were able to perform successful AFM imaging of a standard silicon calibration grating at line rates up to several kHz.

II. PID CONTROLLER IMPLEMENTATION

Proportional, integral and derivative parts of the system, together with summation of their outputs, can be realized in analog electronics by using operational amplifiers and passive components, such as resistors and capacitors placed at the amplifier input and in the feedback loop[33]. In the design of the digitally controlled analog PID, we used this analog design. However, in order to achieve digital control of the gain parameters, some of the resistors were replaced with digital-to-analog converters. These DACs convert digital control data into a certain resistance value using a resistor ladder network. In such an implementation, the user can configure the PID controller gains as well as various other operating parameters using a computer interface. The gain values are then communicated to the PID controller through a digital interface.

In order to achieve a higher frequency range for the integral and the derivative gain stage, these stages were realized as a combination of two gain stages: coarse and fine. In the coarse gain stage, a single integrator or differentiator was chosen to set the coarse gain by choosing one of eight capacitor values. Afterwards, the gain value is fine-tuned by the fine gain stage through an operational amplifier with a digitally controlled resistor ladder network at the input. An image of the PID controller board is presented in Figure 1. A schematic of the digitally controlled analog PID controller is presented in Figure 2(a).

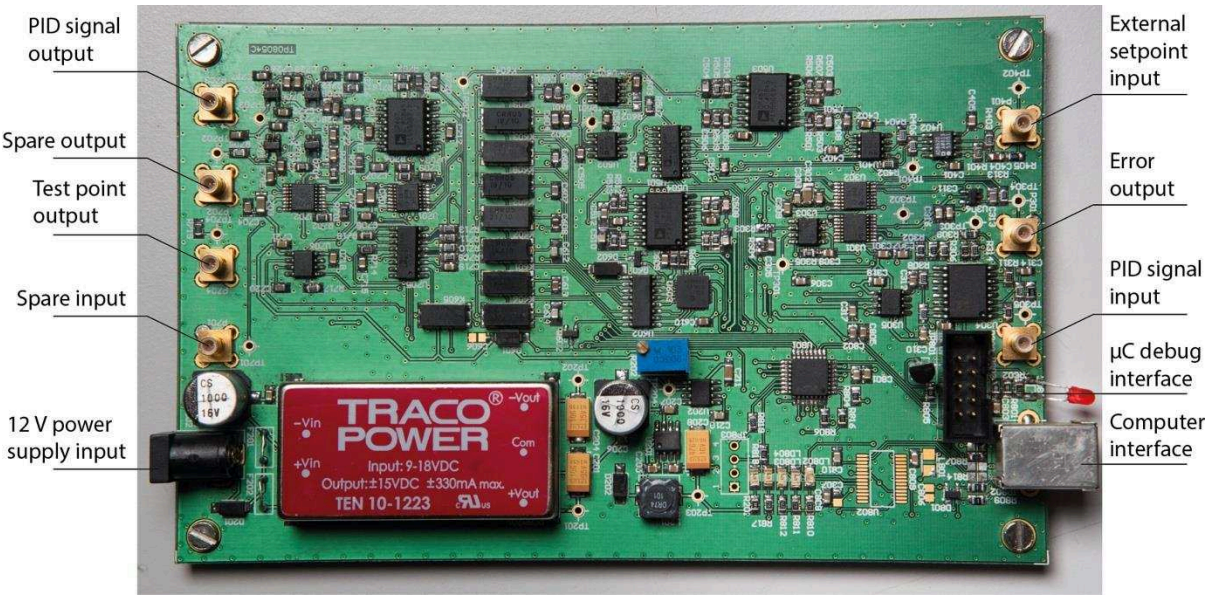

FIG. 1. An image of the PID controller electrical board explaining all input and output interfaces.

A. *Proportional part*

The proportional part has only a fine gain stage implemented (Figure 2(b)). All fine gain stages are implemented using inverting operational amplifiers (OP467GS, Analog Devices, USA). The fine gain is tuned by changing the value of the amplifier's input resistor, which is done through a digitally controlled R-2R resistor ladder network (DAC8812, Texas Instruments, USA). The proportional gain can be tuned up to a gain of 1. The system response of the proportional gain stage at maximum gain setting has a -3 dB bandwidth of about 2 MHz.

B. *Integral part*

The coarse gain of the integral part is defined by an operational amplifier integrator (AD811JR, Analog Devices, USA). The coarse integrator gain is set by choosing the value of the capacitor in the feedback loop. Only one feedback capacitor is closing the feedback at a given time, which is set by an array of reed relay switches (CRR05-1A, Meder electronic Inc, USA), as shown in Figure 2(a). This implementation of the integral part was chosen rather than implementing an array of operational amplifier integrators, in order to prevent overheating of the faster integrators in saturation. The system responses of the 8 coarse integrator gain stages are presented in Figure 2(c). The shaded area roughly represents a fine tuning range

of gains for a selected coarse integrator stage. The noise present in the upper gain range of the integrator characteristics comes from the closed-loop measurement procedure. The characteristics were calculated by simultaneously measuring both the input and the output of each integrator. For the faster integrators, feedback input error at lower frequencies was on par with the lock-in noise.

C. Derivative part

Saturation is not an issue in operational amplifier differentiators. For this reason, the coarse gain of the derivative part is implemented as an array of 8 operational amplifier differentiators (OP467GS, Analog Devices, USA), each one having a different time constant set by a different capacitor value at the input. Further, the coarse gain is set by selecting the output of the chosen differentiator with an analog multiplexer (ADG508, Analog Devices, USA), as presented in Figure 2(a). The system responses of the 8 coarse differentiator gain stages are presented in Figure 2(d). Again, the shaded area roughly represents a fine tuning range of gains for a selected coarse differentiator stage. Due to the fact that the gain of a derivative part increases with frequency, an additional resistor is placed at the differentiator amplifier's input to limit the gain at higher frequencies and hence limit a potential amplification of high frequency noise.

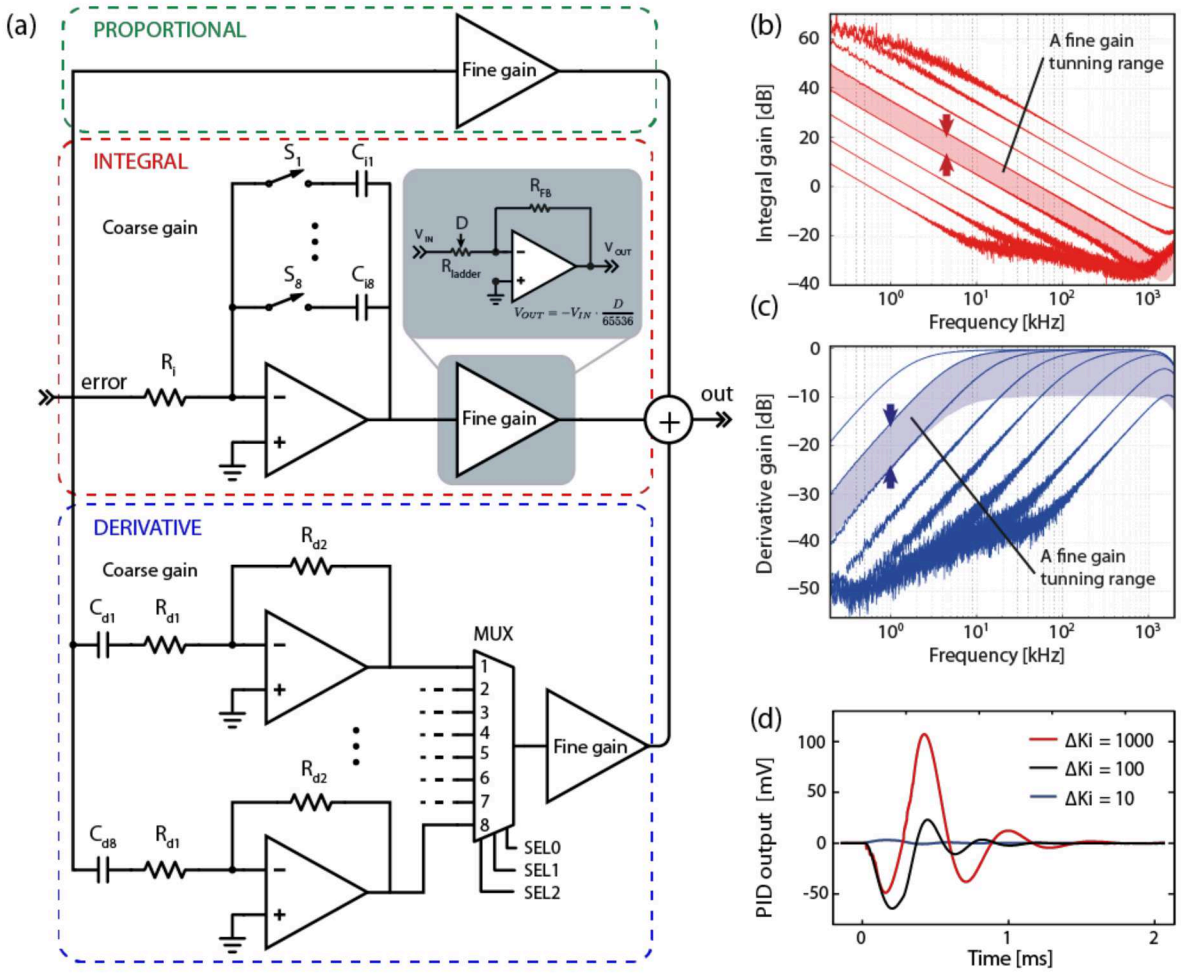

FIG. 2. (a) A schematic of the PID controller design, presenting the coarse and fine gain stages. The fine gain stage is realised using a digitally controlled R-2R resistor ladder network and an inverting operational amplifier. The value of the input resistor, and hence the amplification, is controlled by the 16-bit digital data *D,* according to the equation presented in the figure. (b) Measured responses of the 8 integrator coarse gain stages. The shaded area roughly represents a fine tuning range of gains, for a selected coarse integrator stage, with response characteristic just above the shaded area. (c) Measured responses of the 8 differentiator coarse gain stages. The shaded area roughly represents a fine tuning range of gains for a selected coarse differentiator stage, with response characteristic just above the shaded area. (d) Measured transient voltage resulting from fine and coarse integral gain changes.

D. PID gain adjustment

In standard AFM imaging, gains of the PID controller differ for each imaging experiment and need to be tuned each time. It is a common routine to start imaging and then increase each gain until visible oscillations in the feedback loop occur. Each gain is then set to the maximum value at which no oscillations are visible. As it would be impractical to separately adjust coarse and fine gains during PID operation, continuous integral and derivative gain adjustment was implemented in the software (LabView, National Instruments, USA). Both gains are exponentially increased, such as to provide the fine gain steps at lower gain values and the large gain steps at higher gain values.

III. PID CONTROLER PERFORMANCE CHARACTERIZATION

We characterized our PID controller in terms of electrical bandwidth, output noise and the disturbance rejection sensitivity when the PID controller is placed in an AFM feedback loop. The electrical bandwidth was measured both in open loop (P gain only), Figure 3(c), and in closed loop by sweeping the frequency of the input signal, while the PID output was fed back to the external setpoint input (Figure 3(c)). The gains of the PID controller were increased up to the point where frequency response peaking would start to show and several curves with different gain settings were measured. The amplitude and the phase frequency response of the PID controller, measured under such set gains, are presented in Figure 3(b). The −3 dB bandwidth was measured to be about 834 kHz.

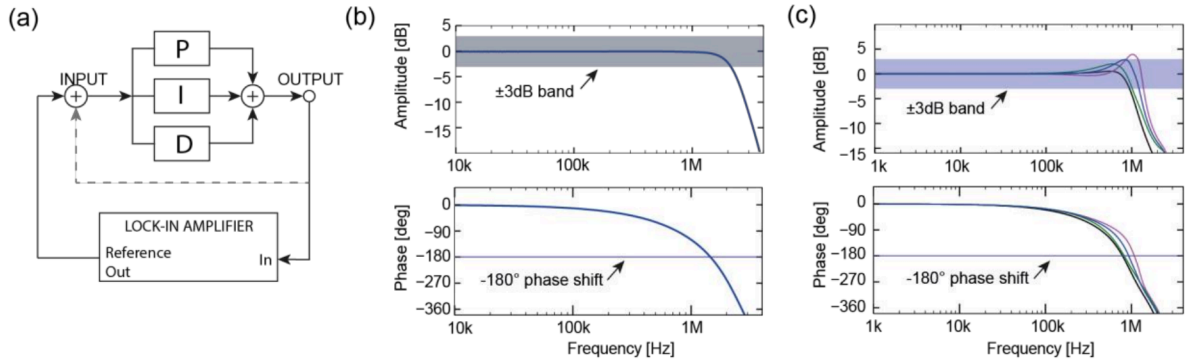

FIG. 3. Electrical bandwidth measurement: (a) A schematic of the measurement setup. Dotted line was connected for closed loop measurement in panel c. (b) Open loop transfer function of the PID with the I and D gains set to zero. The phase drops to 180degr at ca 1.5MHz.(c) Closed loop frequency response of the PID without a plant, showing increasing peaking and higher bandwidth for higher gain settings.

It should be noted from the open loop phase response (see Figure 3(b)) that the phase loss reaches -180° at 1.5MHz, which will limit the closed loop bandwidth (Figure 3(c)). The reason for this is that the current implementation has a large array of operational amplifiers and switches on the signal path, each of them contributing a certain phase delay. This design was implemented in order to provide more options for testing the circuit as well as various functionalities such as an inversion of the input signal, amplification of an error signal and the option to switch off individual gain parts. Simplifying the design of the system by removing some of these options, and therefore decreasing the number of components, would lead to a reduction of the phase loss and a to a better overall performance of the controller.

We also measured the voltage noise spectral density on the PID controller output. The PID controller was connected as shown in Figure 3(a), and gains were increased just up to the point where the frequency response peaking would start to show. The input of the PID controller was terminated with a 50 Ω resistance and the setpoint was set to 0 V. Output noise level of the base line above 100 Hz was typically around 0.2 - 0.4 μV/ √Hz. However, some noise spurs were also present during the measurement. These spurs could be a result of the measurement, the DC/DC converter, or residual crosstalk from the digital logic controlling the R-2R networks..

We tested the performance of our analog PID controller and that of commercial FPGA-based high-speed controllers (Nanoscope V & Nanoscope 3A, Bruker) in an AFM feedback loop (Multimode 8 AFM, Bruker). We measured the disturbance rejection of the PID controller in an AFM feedback loop. We performed a comparison between our analog PID controller and the digital controller present in the standard commercial AFM system, see Figure 4. A sinusoidal height modulation (disturbance) at variable frequency was added to the z-axis controller output and the resulting deflection of the cantilever in contact mode was measured (see Figure 4(a) for measurement setup). A custom made fast z-scanner with a flat response up to around 200 kHz, a custom made high-speed high-voltage piezo amplifier[34] and a custom-built AFM head[35,36] were used in the measurements. The gains of both PID controllers were increased up to the point where visible oscillations of the system would start to show in the AFM image or up the point where there was no visible frequency response peaking present in the closed-loop response. Figure 4(b) shows the disturbance rejection sensitivity for both cases. The disturbance rejection sensitivity is a measurement of the residual error when the controller tracks topography changes at different frequencies.

With increasing frequency of the disturbance, the PID controller will stop reacting fast enough to produce an appropriate signal to cancel the cantilever deflection error. At that point, the cantilever deflection error starts to rise. Finally, past a certain frequency, the PID controller will not track the surface at all and the entire height disturbance will be present in the cantilever deflection error. From Figure 4(b) we see that the analog PID controller rejects the height disturbances at frequencies up to one order of magnitude higher than the digital PI controller.

The resonance peak at around 300 kHz is resonance of the z-scanner. The peaking in the response measured just before visible oscillations in an AFM image occur (dashed lines in Figure 4.) comes from the fact that we increased the gains to the point where the system becomes unstable. The frequency of the peaks, and hence the bandwidth of the closed-loop feedback is determined by the combined delays of various components in the AFM feedback loop: scanner, deflection readout, PID controller and high-voltage amplifier.

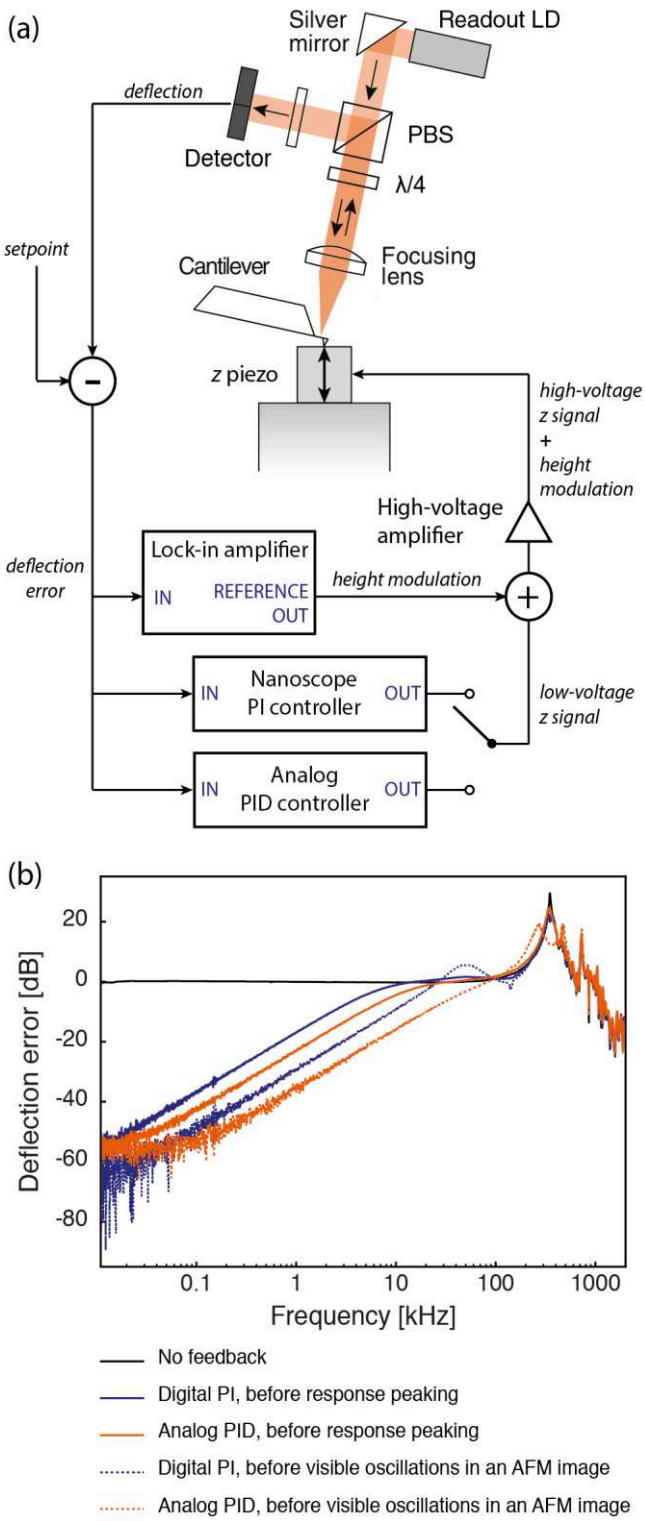

FIG. 4. Comparison of the closed loop disturbance rejection sensitivity between the presented analog PID and the standard commercial digital controller in cantilever surface tracking: (a) Measurement setup. (b) The measured disturbance rejection sensitivity measures the ability of the controller to track topographic changes at different frequencies. The proposed analog PID controller (red) is almost an order of magnitude faster than the commercial digital PI controller (blue) for the same measurement conditions.

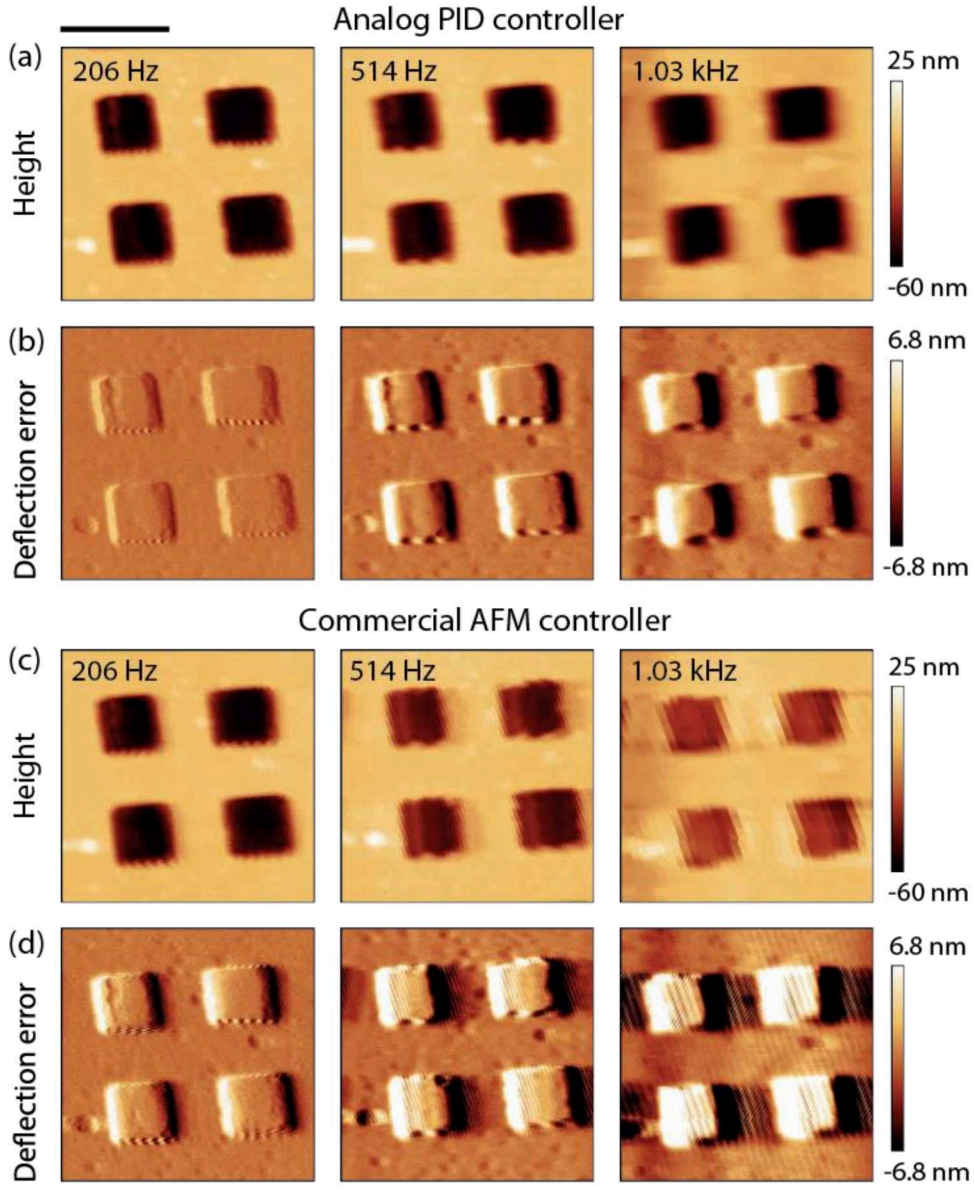

FIG. 5. A comparison of HS-AFM imaging between the analog PID and the standard commercial digital controller. a) The tracking performance of the analog PID decreases with increasing line rate, but the pits of the calibration standard are still clearly resolved in depth when scanning at 1030 lines/s. b) The deflection error image shows IV.that the controller manages to descend into the pits reproducibly and quickly. c) In comparison to the analog PID, the commercial digital controller quickly degrades in tracking performance and shows noticeable quantisation artifacts. d) Even at 514 lines/s the commercial controller does not manage to descend into the pits anymore, and at 1030 lines/s the tracking degrades enough that the height of the pits is severely distorted.

V. HIGH-SPEED AFM IMAGING PERFORMANCE

We used the analog PID controller to perform HS-AFM imaging in contact mode, using a soft cantilever probe in air (spring constant of 0.4N/m and resonance frequency of 70kHz).The imaging was performed with a custom made AFM high-speed scanner, similar to the one published in[13,14] and a custom-built AFM head[37]. The AFM image acquisition was performed with a custom made data acquisition system[13,38]. We used a commercial high-speed AFM

piezoamplifier (Techproject EMC, Austria) for driving the slow axis piezos of the scanner. For driving the fast axis and the z-piezo, a custom made high-speed high-voltage piezo amplifier was used[39]. We used a silicon calibration grating (1 µm × 1 µm, 50 nm deep) as a sample to test the HS-AFM imaging performance of the analog PID controller.

Figure 5. shows a comparison of HS-AFM images obtained using the analog PID controller and the digital controller present in the standard commercial AFM. The images were taken at 206 Hz, 514 Hz and 1.03 kHz line rates. For both controllers, the gains were set just below the point where oscillations in the feedback loop would appear. From the deflection error images, one can notice that the analog PID was tracking the sample surface significantly better at all speeds. The commercial AFM PI controller is also limited in the sampling speed of its analog-to-digital and digital-to-analog converters, which makes images look increasingly pixelated at higher scanning speeds. The sampling rate of the commercial PI was measured to be around 60 kHz.

During AFM imaging, the gains need to be often adjusted to obtain an optimal AFM image. In our digitally controlled analog PID, small gain changes (changes in the R-2R ladder) result in only minor transients which settle down quickly during imaging. Larger changes (switching gain ranges) however cause moderately high transients. Even in the worse switching configurations (corse integral changes), these transients do not damage the AFM tip as the amplitude of the Z-piezo perturbation they generate is well below 20nm.

In order to test the worst case, we performed a 1000x gain change (from *Ki* = 1 to *K*i = 1000), including both resistor network switching as well as coarse gain switching, see the red line below. This large change did induce a significant swing in the output voltage of the PID and thus on the piezo control voltage (as is to be expected). Nevertheless, even for this extreme gain change, the output voltage swing is only about 150mV which, after amplification, corresponds to an actual displacement of the Z-piezo of less than 20nm. Fortunately, this is not sufficient to damage the AFM tip.

The comparison shows the potential to improve the feedback controller bandwidth if we want to reach kHz line rates. While at few 100s of Hz/s line rates a commercial digital feedback controller could still track the sample (see Figure 5, at 206 Hz and 512 Hz line rates) – at 1 kHz line rate the tracking with our existing digital controller is not possible (see Figure 5, at 1.03 kHz line rates). It should be noted, however, that by using higher speed D/A converters and more powerful digital processors it would be possible to increase the feedback bandwidth as well. The efforts to increase the feedback bandwidth to the level of the analog PID, however, are significantly more than what is needed to add digital control to an analog PID.

VI. DISCUSSION AND CONCLUSION

Due to signal sampling and aliasing issues, digital PID controllers must operate at frequencies that are 10-20 times higher than the closed loop bandwidth of the overall control loop. On the other hand, analog controllers do not face such issues and should be able to provide much faster response. Previously, due to the lack of the possibility to adjust control parameters at run-time, analog PID controllers were mostly used in control of invariable processes, where the desired control gains were determined and set by fixed components to never or rarely change. Implementing digital control of the analog controller parameters opens up new possibilities for the use of analog PID controllers, which can be especially beneficial for the control of fast processes.

One of the benefits of digital controllers is that they can be easily reconfigured (e.g. to include or exclude some gain parameters or to change the PID configuration from parallel to serial etc.). In our analog PID controller, we enabled a user to include or exclude some of the PID gains by using analog switches. However, the switches introduce additional phase loss on the signal path and limit the controller bandwidth.

Although the derivative part of the feedback controller is usually omitted in standard AFM systems due to the fact that it amplifies high frequency noise, we performed AFM imaging with and without the derivative part (derivative gain was set to almost zero) and we found that the derivative part still helped to slightly improve the image quality and tracking.

We developed a digitally controlled analog PID controller and successfully demonstrated that it can be used in high-speed AFM imaging at several kHz line rates and several mm/s surface speed. The current design of the PID controller could be improved in terms of bandwidth and phase loss by simplifying the design and removing some of the components in the signal path, and by replacing some components for ones with a faster performance. We think that the noise of the system could also be improved by a redesign, for instance by replacing the switching DC/DC converter power supply currently being used.

ACKNOWLEDGEMENTS

This work has been funded by the European Union's Seventh Framework Programme FP7/2007-2011 under grant 286146, by the European Union FP7/2007-2013/ERC under Grant Agreement No. 307338-NaMic, and Eurostars Eurostars E!8213-TripleS. C.Y. acknowledges the financial support from the China Scholarship Council for his joint PhD project (Grant No.201306120115).

[1] A.J. Katan and C. Dekker, Cell **147**, 979 (2011).

[2] T. Ando, Nanotechnology **23**, 62001 (2012).

[3] N. Kodera, D. Yamamoto, R. Ishikawa, and T. Ando, Nature **468**, 72 (2010).

[4] G.E. Fantner, R.J. Barbero, D.S. Gray, and A.M. Belcher, Nat. Nanotechnol. **5**, 280 (2010).

[5] I. Casuso, P. Sens, F. Rico, and S. Scheuring, Biophys. J. **99**, L47 (2010).

[6] T. Uchihashi, R. Iino, T. Ando, and H. Noji, Science **333**, 755 (2011).

[7] M. Imamura, T. Uchihashi, T. Ando, A. Leifert, U. Simon, A.D. Malay, and J.G. Heddle, Nano Lett. **15**, 1331 (2015).

[8] M.B. Viani, T.E. Schäffer, A. Chand, M. Rief, H.E. Gaub, and P.K. Hansma, J. Appl. Phys. **86**, 2258 (1999).

[9] M. Kitazawa, K. Shiotani, and A. Toda, Japanese J. Appl. Physics, Part 1 Regul. Pap. Short Notes Rev. Pap. **42**, 4844 (2003).

[10] J.D. Adams, B.W. Erickson, J. Grossenbacher, J. Brugger, A. Nievergelt, and G.E. Fantner, Nat. Nanotechnol. **11**, 147 (2015).

[11] T. Ando, N. Kodera, E. Takai, D. Maruyama, K. Saito, and A. Toda, Proc. Natl. Acad. Sci. U. S. A. **98**, 12468 (2001).

[12] A.D.L. Humphris, M.J. Miles, and J.K. Hobbs, Appl. Phys. Lett. **86**, 34106 (2005).

[13] G.E. Fantner, G. Schitter, J.H. Kindt, T. Ivanov, K. Ivanova, R. Patel, N. Holten-Andersen, J. Adams, P.J. Thurner, I.W. Rangelow, and P.K. Hansma, Ultramicroscopy **106**, 881 (2006).

[14] G. Schitter, K.J. Astrom, B.E. DeMartini, P.J. Thurner, K.L. Turner, and P.K. Hansma, IEEE Trans. Control Syst. Technol. **15**, 906 (2007).

[15] C. Braunsmann and T.E. Schäffer, Nanotechnology **21**, 225705 (2010).

[16] A.P. Nievergelt, B.W. Erickson, N. Hosseini, J.D. Adams, and G.E. Fantner, Sci. Rep. **5**, 11987 (2015).

[17] C. Yang, J. Yan, M. Dukic, N. Hosseini, J. Zhao, and G.E. Fantner, Scanning **9999**, 1 (2016).

[18] B. Schlecker, M. Dukic, B. Erickson, M. Ortmanns, G. Fantner, and J. Anders, IEEE Trans.

Biomed. Circuits Syst. **8**, 206 (2014).

[19] V. Aggarwal, Meng Mao, and U.-M. O'Reilly, in *First NASA/ESA Conf. Adapt. Hardw. Syst.* (IEEE, 2006), pp. 12–19.

[20] Yifan Sun, Y. Fang, Yudong Zhang, and Xiaokun Dong, in *2010 IEEE Int. Conf. Control Appl.* (IEEE, 2010), pp. 245–250.

[21] G. Schitter, P. Menold, H.F. Knapp, F. Allgower, and A. Stemmer, Rev. Sci. Instrum. **72**, 3320 (2001).

[22] S. Salapaka, A. Sebastian, J.P. Cleveland, and M. V. Salapaka, Rev. Sci. Instrum. **73**, 3232 (2002).

[23] N. Chuang, in *2014 Australas. Univ. Power Eng. Conf.* (IEEE, 2014), pp. 1–6.

[24] Hiroshi Fujimoto and Takashi Oshima, in *2008 10th IEEE Int. Work. Adv. Motion Control* (IEEE, 2008), pp. 568–573.

[25] Ying Wu, Qingze Zou, and Chanmin Su, in *2008 Am. Control Conf.* (IEEE, 2008), pp. 2040–2045.

[26] U. Aridogan, Y. Shan, and K.K. Leang, J. Dyn. Syst. Meas. Control **131**, 61103 (2009).

[27] S. Necipoglu, S. a. Cebeci, Y.E. Has, L. Guvenc, and C. Basdogan, IEEE Trans. Nanotechnol. **10**, 1074 (2011).

[28] I. Lita, D.A. Visan, and I.B. Cioc, in *2009 32nd Int. Spring Semin. Electron. Technol.* (IEEE, 2009), pp. 1–4.

[29] G. Schitter and N. Phan, in *2008 Am. Control Conf.* (IEEE, 2008), pp. 2690–2695.

[30] Y.K. Yong, B. Bhikkaji, and S.O.R. Reza Moheimani, IEEE/ASME Trans. Mechatronics **18**, 1060 (2013).

[31] Anadigm, Chapter 9: AnadigmPID (2004).

[32] N. Kodera, M. Sakashita, and T. Ando, Rev. Sci. Instrum. **77**, 83704 (2006).

[33] R. Ugodzinski, R. Szewczyk, and M. Nowicki, Filev D. Al. Intell. Syst. Adv. Intell. Syst. Comput. **323**, 89 (2015).

[34] A.P. Nievergelt, S.H. Andany, J.D. Adams, M.T. Hannebelle, and G.E. Fantner, IEEE/ASME Int. Conf. Adv. Intell. Mechatronics, AIM **Accepted**, (2017).

[35] J.D. Adams, A. Nievergelt, B.W. Erickson, C. Yang, M. Dukic, and G.E. Fantner, Rev. Sci. Instrum. **85**, (2014).

[36] A.P. Nievergelt, J.D. Adams, P.D. Odermatt, and G.E. Fantner, Beilstein J. Nanotechnol. **5**, 2459 (2014).

[37] J.D. Adams, C.H. Schwalb, M. Winhold, M. Đukić, M. Huth, and G.E. Fantner, Proc. SPIE Microtechnologies, Smart Sensors, Actuators, MEMS **8763**, 876327 (2013).

[38] G.E. Fantner, P. Hegarty, J.J.H. Kindt, G. Schitter, G.A.G. Cidade, and P.K. Hansma, Rev. Sci. Instrum. **76**, 26118 (2005).

[39] S. Andany, A.P. Nievergelt, M. Dukic, and G.E. Fantner, in *Int. Scanning Probe Microsc. Conf.* (Grindelwald, 2016).